

COLLIMATION OF ASTROPHYSICAL JETS: THE PROTO-PLANETARY NEBULA He 3-1475

KAZIMIERZ J. BORKOWSKI AND JOHN M. BLONDIN

Department of Physics, North Carolina State University, Raleigh, NC 27695

AND

J. PATRICK HARRINGTON

Department of Astronomy, University of Maryland, College Park, MD 20742

Received 1997 February 11; accepted 1997 March 19

ABSTRACT

The proto-planetary nebula He 3-1475 was imaged in the [N II] $\lambda 6584$ line with the Wide Field Planetary Camera 2 on board the *Hubble Space Telescope*. This image has revealed what appear to be large-scale flows being collimated into narrow bipolar jets. This is a unique object: we may be observing the actual collimation process of an astrophysical jet. Analytical models and hydrodynamical simulations suggest that the jet in He 3-1475 may be produced by purely hydrodynamical means, through focusing of a weakly collimated bipolar outflow into jets by oblique radiative shocks.

Subject headings: hydrodynamics — ISM: jets and outflows — planetary nebulae: individual (He 3-1475) — shock waves

1. ASTROPHYSICAL JETS AND THEIR COLLIMATION

Jets are ubiquitous in astrophysical flows. They are found around young stellar objects, around evolved mass-losing stars, and in planetary nebulae. They seem easily produced by compact objects such as neutron stars or black holes in galactic nuclei. Yet their origin is shrouded in mystery, primarily because jets seem to originate in small-scale structures that are difficult to observe. Despite decades of intense efforts, there is not even one example of a jet whose origin is clearly understood. Collimation of jets is one of the most urgent, unsolved problems in astrophysics.

It is usually assumed that accretion onto a central object, such as a young star surrounded by its circumstellar debris or a stellar companion in a binary system, is a necessary prerequisite for jet collimation. But is accretion really necessary? And irrespective of the answer to this question, are magnetic fields necessary to collimate jets, as has been often assumed? Or is it possible to produce astrophysical jets by purely hydrodynamical means? This is an active research area in theoretical astrophysics, with an extensive literature and with many possibilities (e.g., see a discussion on jets associated with young stellar objects by Frank & Mellema 1996). The main difficulties arise from flow complexities and lack of suitable observational data.

We recently acquired a *Hubble Space Telescope* (*HST*) image of the proto-planetary nebula He 3-1475 exhibiting tantalizing fine-scale morphological features that suggest purely hydrodynamical collimation of its jets. We report here on this discovery and present hydrodynamical models supporting this suggestion.

2. JETS IN THE PROTO-PLANETARY NEBULA He 3-1475

He 3-1475 is a Be star (Henize 1976), recently identified as a rare object making the transition from a dust-enshrouded asymptotic giant branch (AGB) star to a planetary nebula (PN). The star is surrounded by an expanding (12 km s^{-1}) torus of molecular material, seen through its CO emission (Knapp et al. 1995). This torus intercepts most of the stellar

radiation, reradiating it through the far-infrared thermal dust emission (Parthasarathy & Pottasch 1989). Strong near-IR Ca II emission lines and permitted and forbidden Fe II emission lines (Riera et al. 1995) most likely originate in the warm and dense neutral gas produced by photodissociation of the molecular torus by the central star. He 3-1475 exhibits OH maser emission (te Lintel Hekkert 1991; Bobrowsky et al. 1995), which is seen in a number of proto-PNs (PPNs) and young PNs (Zijlstra et al. 1989; te Lintel Hekkert & Chapman 1996). Both CO and OH emission-line profiles have a broad (60 km s^{-1}) component indicative of a fast molecular outflow associated with the torus, which appears to be spatially extended ($2''$ in size). Such fast molecular outflows and associated tori are seen in a number of post-AGB stars. In particular, spatiokinematical properties of OH emission in He 3-1475 and in the post-AGB star HD 101584 are very similar (te Lintel Hekkert et al. 1992).

Recent observations with the VLA revealed the presence of a compact, unresolved PN close to the star (Bobrowsky et al. 1995; Knapp et al. 1995). Apparently, the central star became hot enough to ionize gas in its vicinity, which is consistent with its early (B) spectral type. The PN age is uncertain, but it may be only 15 yr (Knapp et al. 1995). The optical spectrum of the star shows strong P Cygni Balmer line profiles (Riera et al. 1995), which indicates mass outflows with velocities as high as 700 km s^{-1} . These observations indicate that the central star is currently undergoing transition from the AGB stage to the PN stage, an important and poorly understood juncture in stellar evolution. Among similar post-AGB objects with OH maser emission, He 3-1475 is the intermediate case between older, less compact young planetary nebulae such as Vy 2-2 (Seaquist & Davis 1983) and cooler stars such as HD 101584 (Bakker et al. 1996) and M1-92 (Solf 1994).

The most spectacular features in He 3-1475 are its optical jets (Riera et al. 1995; Bobrowsky et al. 1995). Ground-based images taken through narrowband $H\alpha$ filters showed three pairs of symmetric knots located at slightly different position angles but in the direction perpendicular to the molecular torus. Because knots are symmetric with respect to the central

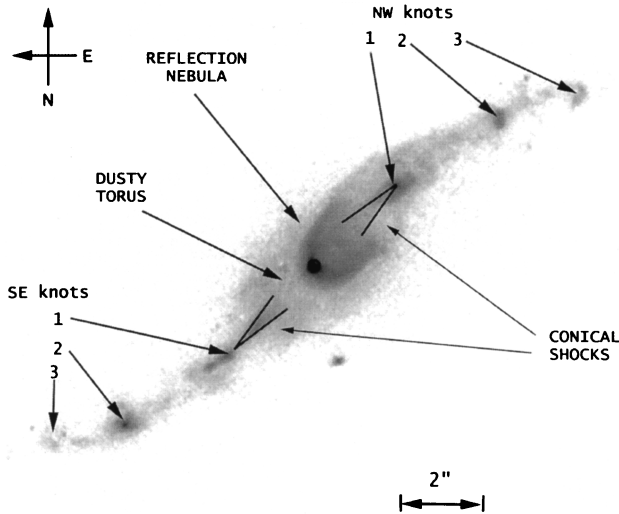


FIG. 2.—Sketch of He 3-1475 with various morphological features indicated (see text for explanation).

star, this symmetry is commonly referred to as point symmetry. High- and medium-resolution ground-based spectroscopy revealed that outer pairs of knots move away from the central star with radial velocities of 500 km s^{-1} . Closer to the star, Riera et al. (1995) found jetlike outflows with radial velocities as high as 850 km s^{-1} with respect to the central star. Strong [O I] $\lambda\lambda 6300, 6464$, [N II] $\lambda\lambda 6548, 6584$, and [S II] $\lambda\lambda 6717, 6731$ emission lines and large (up to 450 km s^{-1}) widths of $H\alpha$ and forbidden lines indicate shocks as the excitation mechanism for the observed emission. Riera et al. (1995) found shock velocities of $\sim 100 \text{ km s}^{-1}$, using observed [O III] $\lambda 5007/H\alpha$ line ratios. In such intermediate-velocity shocks, the postshock gas cools rapidly so that shocks in He 3-1475 must be radiative shocks.

3. HUBBLE SPACE TELESCOPE IMAGING

In cycle 6 of the *HST* guest observer program we began a snapshot survey for jets in PNs, and He 3-1475 was the first target imaged with the Wide Field Planetary Camera (WFPC2). Two exposures through the F658N filter encompassing the [N II] $\lambda 6584$ emission line, 200 s and 400 s in duration, were obtained on 1996 June 26, with He 3-1475 located entirely on the PC chip. These images went through the standard pipeline processing at the Space Telescope Science Institute, and then the Space Telescope Science Data Analysis Software task “crrej” was used to remove cosmic rays and combine these images into the result shown in Figure 1 (Plate L5).

The brightest region at the center of Figure 1 contains a U-shaped, limb-brightened reflection nebula, with the central star of He 3-1475 located at its bottom (see also the sketch in Fig. 2). This morphology is consistent with previous WFPC1 *HST* images (Bobrowsky et al. 1995) obtained with the aberrated telescope through the F487N and F502N filters. The total (the reflection nebula plus the central star) count rate is $410 \text{ counts s}^{-1}$, which gives the continuum flux of $4.4 \times 10^{-14} \text{ ergs cm}^{-2} \text{ s}^{-1} \text{ \AA}^{-1}$. (A strong stellar $H\alpha$ line may also contribute to the observed count rate.) The surface brightness of the reflection nebula changes smoothly from $3.9 \times 10^{-15} \text{ ergs cm}^{-2} \text{ s}^{-1} \text{ \AA}^{-1} \text{ arcsec}^{-2}$ at the top of the nebula (about $1''.5$ from the star) to the value 1 order of magnitude larger close to the star.

The stellar image appears to be somewhat asymmetric, which suggests an enhancement in the surface brightness of the reflection nebula close to the central star. At most one-fifth of the total flux is contained in the central star, which implies that we see the star through at least 2 mag of extinction internal to the nebula.

Figure 1 reveals a faint southeastern counterpart to the bright U-shaped reflection nebula in the northwest. This counterpart is located behind a dusty molecular torus depicted in Figure 6 of Bobrowsky et al. (1995) and suffers a substantial (2–3 mag) extinction within the torus. The densest part of the torus is clearly seen in Figure 1: it is present in absorption southeast from the star and appears in reflection to the northwest, with a total spatial extent of $2''$. The $2''$ size of the torus coincides with the size of the OH maser emission, and the OH emission is blueshifted in the southeast and redshifted in the northwest, which strongly suggests that the torus seen in the *HST* image is indeed associated with the maser emission. If we assume a standard interstellar extinction law and a standard interstellar medium (ISM) dust content, 2.5 mag of extinction at $\lambda 6584$ corresponds to the hydrogen column density $N_{\text{H}} = 6 \times 10^{21} \text{ cm}^{-2}$. At an assumed distance of 2 kpc, the $1''$ radius of the torus corresponds to $3 \times 10^{16} \text{ cm}$, which implies an average torus density of $\sim 2 \times 10^5 \text{ cm}^{-3}$. Several dark patches appear in the torus in the south and southeast, which suggests the presence of opaque clumps containing even denser material.

Our [N II] *HST* image clearly shows three pairs of symmetric, high-velocity emission knots, which were first detected through ground-based observations (Bobrowsky et al. 1995; Riera et al. 1995). Emission knots to the northwest are blueshifted and those to the southeast are redshifted, which implies outflows perpendicular to the torus. These knots are very well collimated with the central star: the star is only $0''.027$ from a line connecting the innermost pair of knots, located at $2''.84$ NW and $2''.97$ SE from the star. Likewise, the line connecting the middle pair of knots ($5''.83$ NW and $5''.92$ SE from the star) is only $0''.048$ (just over one $0''.0455$ PC pixel) from the star. But these pairs of emission knots are located at different position angles: the innermost pair at P.A. $135^\circ 07'$ and the middle pair at P.A. $129^\circ 21'$, and the outermost pair (at $7''.82$ NW and $7''.57$ SE from the star) is displaced an additional $5^\circ 33'$ from the middle pair. The presence of such pairs of compact emission features at different position angles is the signature of point symmetry, and He 3-1475 belongs to a small but important group of point-symmetric PNs and PPNs.

All emission knots are clearly extended, but the innermost pair of knots and the southeastern knot of the middle pair possess stellar-like cores that may be unresolved. We measure the following [N II] $\lambda 6584$ fluxes (in $\text{ergs cm}^{-2} \text{ s}^{-1}$) through a $1''$ diameter aperture: innermost northwestern and southeastern knots, 1.97×10^{-13} and 7.61×10^{-14} ; middle knots, 5.09×10^{-14} and 9.30×10^{-14} ; and 1.25×10^{-14} and 1.05×10^{-14} for the fainter outermost knots. The quoted fluxes for the knots in the southeast are likely to be underestimated because we did not take into account the reduced transmission of the F658N filter for these highly ($\sim 500 \text{ km s}^{-1}$) redshifted knots. We note that our [N II] $\lambda 6584$ line fluxes for the middle pair of knots are more than 1 order of magnitude larger than those given by Riera et al. (1995) for their “northwestern” and “southeastern” (actually southeastern and northwestern) knots.

The most remarkable features in our *HST* image are thin converging lines ending in the innermost pair of knots. Be-

cause the [N II] emission in He 3-1475 is produced by shock excitation (Bobrowsky et al. 1995; Riera et al. 1995), these lines mark the location of converging shocks, most likely the limb-brightened edges of conical shocks. These shocks can be traced close to the central star in the blueshifted (approaching) northwestern lobe of the bipolar outflow, until they are lost against the glare of the torus seen in the reflected light. Their average collimation angle in the northwestern lobe is about 25° , but they are clearly curved and may even be converging onto the central star. In the redshifted (southeastern) lobe of the outflow, these shocks emerge from behind the obscuring torus $1''$ from the star, $0''.5$ apart and with a collimation angle of 20° . In both lobes, converging shocks merge about $0''.5$ before the innermost emission knots, forming well-defined jets seen most clearly in the southeast. The jets are not radial, e.g., the southeastern jet is inclined by about 12° with respect to the radial direction. It is not clear whether this deviation from the radial direction occurs entirely at the beginning of the jet, at the vertex of conical shocks, or whether further bending occurs at the innermost knots.

The high-velocity jets in He 3-1475 do not appear to originate in the vicinity of the central star. Instead, on the basis of the morphological evidence described above, we identify the conical converging shocks in our *HST* image as the jet collimation region. As we discuss next, this collimation may be achieved through purely hydrodynamical means involving radiatively cooling shocks.

4. HYDRODYNAMICAL MODELS OF JET COLLIMATION

The conical converging shocks, such as those seen in Figure 1, have been predicted in hydrodynamical models of jet collimation involving oblique shocks. The simplest example is provided by a steady state, initially poorly collimated outflow expanding into an ambient medium with thermal pressure P (which may vary spatially). In these thermal pressure confinement models (Cantó 1980; Eichler 1982; Smith 1985), supersonically moving gas enters an oblique shock, which focuses the outflow onto the vertex of a cone pointing along the symmetry axis of the outflow. The collimation is completed at the vertex, where the conical converging flow is transformed into a well-collimated jet (Cantó, Tenorio-Tagle, & Różyńska 1988; Tenorio-Tagle, Cantó, & Różyńska 1988). This collimation mechanism usually requires the shocked gas to be radiative. In view of the striking similarity between Figure 1 and the conical flows presented by Cantó (1980), Eichler (1982), and Smith (1985), the thermal pressure confinement model clearly appears to be an attractive explanation. We investigate this model in more detail through hydrodynamical simulations.

In order to better understand our hydrodynamical simulations, we constructed analytical models for the jet collimation mechanism discussed above. These models are similar to those considered by Cantó (1980), Eichler (1982), and Smith (1985), but instead of considering pressure balance at oblique shocks as these authors did, we derived the governing differential equations from conservation of the momentum flux. We present these equations for the case in which the pressure of the ambient medium varies as $r^{-\alpha}$, where r denotes the radial distance from the star and $\alpha < 2$. Distances are measured in units of r_0 , the radial distance at which the ram pressure of the undisturbed stellar wind with the constant mass-loss rate \dot{M}_w and the wind speed v_w is equal to the thermal pressure of the ambient medium. Let θ be the angle between the x -axis and

the radius vector ($\theta = \pi/2$ is the outflow direction). The shock shape $r(\theta)$ is then governed by the following set of three differential equations:

$$\frac{dr}{d\theta} = r \frac{\Phi_r}{\Phi_\theta}, \quad (1)$$

$$\frac{d\Phi_r}{d\theta} = \frac{1}{2} (1 - r^{2-\alpha}) \cos \theta + \Phi_\theta, \quad (2)$$

$$\frac{d\Phi_\theta}{d\theta} = \frac{1}{2} r^{2-\alpha} \cos \theta \frac{\Phi_r}{\Phi_\theta} - \Phi_r, \quad (3)$$

where Φ_r and Φ_θ are components of momentum flux of the shocked stellar wind gas in the coordinate system (r, θ) . These momentum components are in units of $\dot{M}_w v_w$. The shocked stellar wind gas layer is assumed to be geometrically thin, a crucial assumption valid only for radiative shocks. For an outflow with opening angle $\pi - 2\theta_0$ at $r = 0$ and $\theta - \theta_0 \ll 1$, equations (1)–(3) give $r = [(3 - \alpha)(2 - \alpha)(\theta - \theta_0)^2/2]^{1/(2-\alpha)}$, $\Phi_\theta = r^{2-\alpha} \cos \theta_0 / 2(3 - \alpha)$, and $\Phi_r = [\Phi_\theta \cos \theta_0 / (2 - \alpha)]^{1/2}$. Starting with this expansion, the shock shape can now be found by numerical integration of equations (1)–(3) to $\theta = \pi/2$.

Our simulations were computed with VH-1, a time-dependent hydrodynamics code based on the piecewise parabolic method of Colella & Woodward (1984). We assumed axisymmetry, running the models on a two-dimensional cylindrical $(r - z)$ grid with 200×400 zones and an initial jet radius of 32 zones. The gas was treated as an ideal fluid with a ratio of specific heats $\gamma = 5/3$. Radiative energy losses were included on the basis of the interstellar cooling curve of Sutherland & Dopita (1993), although we note that for the low shock velocities present in this simulation, the actual cooling rate may be much higher than we have assumed. The outflow was initialized with a full opening angle of 90° and a velocity of 400 km s^{-1} at a distance of $0.19r_0$ from the source. The mass-loss rate in this outflow was chosen to be large enough to produce rapidly cooling oblique shocks in the collimation region. Note that this condition depends not only on the density of the outflow but also on the outflow velocity, the form of the cooling function, and the length scale of the collimation.

Figure 3 illustrates the structure of the flow after the jet has settled into a quasi-steady equilibrium. The diverging outflow is continually collimated into a narrow jet moving downstream with velocities of order $\sim 350 \text{ km s}^{-1}$. The thin, dense shell associated with the oblique radiative shocks is in good agreement with the shock position given by the analytic model. A slightly larger opening angle (105°) is used for the analytic model to account for the fact that we start the simulation at a finite distance from the source. This simulation suggests that the focusing shock is dynamically unstable, as one might expect in the presence of rapid cooling, thin shells, and strong shear. This instability does not alter the formation of a jet, but it does affect the appearance of the collimating shocks. Most of our simulations exhibited a standing shock in the diverging wind, as can be seen in Figure 3. However, this and other aspects of the simulation may be affected by the forced axisymmetry. In particular, in a three-dimensional simulation, the jet might wobble because of hydrodynamical instabilities and/or an asymmetry of the confining medium. Such a wobbling jet could produce symmetric pairs of knots such as those seen in He 3-1475.

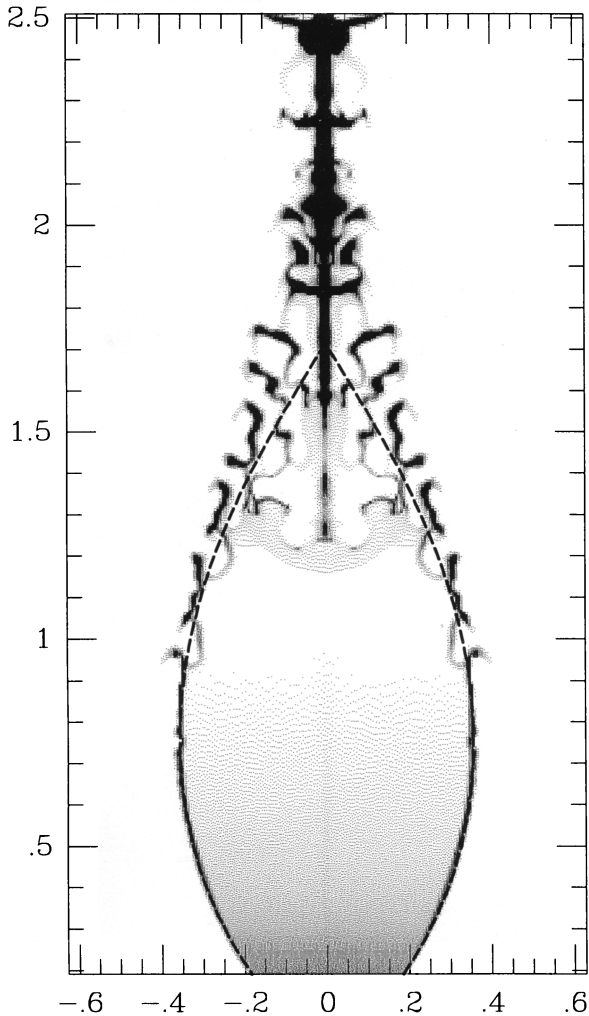


FIG. 3.—Numerical simulation showing hydrodynamic collimation of a diverging supersonic flow. Dimensions are labeled in units of r_0 , defined in the text. The shading represents gas density, with dark regions corresponding to the densest regions of the flow, namely, the cold gas produced behind radiative shocks. The thin shell of cold, dense gas begins to break up because of dynamical instabilities as the flow is collimated onto the symmetry axis. The dashed line outlines the position of the collimating shock in the analytic model described in the text.

Our hydrodynamical simulations demonstrate that jets are likely to form in momentum-driven interactions between stellar outflows and the ambient medium, provided that there is an initial asymmetry either in the stellar wind or in the ambient medium. However, for fast ($\sim 700 \text{ km s}^{-1}$) outflows such as those seen in He 3-1475, jets form in our simulations only at unrealistically high mass-loss rates and high thermal pressures in the confining medium, because only under these conditions do oblique shocks become radiative. This failure suggests that a simple steady state model, in which the outflow is confined by the thermal pressure of the ambient medium, is not appropriate for He 3-1475. Indeed, there is no particular reason why jet formation should take place only in this simple model. For example, Frank, Balick, & Livio (1996) considered an analytic model for the formation of ansae and jets in PNs involving oblique radiative shocks that does not rely on the thermal pressure confinement by the ambient medium. In the case of He 3-1475, conical shocks might not be stationary structures. If they were moving through the ambient medium, its ram pressure could easily exceed its thermal pressure, resulting in an inertial confinement instead of thermal confinement of the outflow. This is a likely possibility because ram pressure of even slow (several tens of kilometers per second) shocks is orders of magnitude higher than the thermal pressure of the relatively cold ($T \leq 1000 \text{ K}$) neutral circumstellar gas in He 3-1475. Hydrodynamical simulations of momentum-driven, time-dependent flows are necessary to investigate under what conditions outflows are collimated into jets by oblique shocks. He 3-1475 offers a unique opportunity for testing these models. Future high spatial and spectral resolution observations of He 3-1475 should provide us with a wealth of information about physical conditions and about shock dynamics in the collimation region and in the confining medium. Because of small spatial scales, these observations are possible only with the *HST*, but they will at last provide us with key data on the collimation of an astrophysical jet.

Support for this work was provided by NASA through grant GO-06347.01-95A from the Space Telescope Science Institute, which is operated by Association of Universities for Research in Astronomy, Inc., under NASA contract NAS5-26555.

REFERENCES

- Bakker, E. J., Lamers, H. J. G. L. M., Waters, L. B. F. M., Waelkens, C., Trams, N. R., & van Winckel, H. 1996, *A&A*, 307, 869
 Bobrowsky, M., Zijlstra, A. A., Grebel, E. K., Tinney, C. G., te Lintel Hekkert, P., Van de Steene, G. C., Likkell, L., & Bedding, T. R. 1995, *ApJ*, 446, L89
 Cantó, J. 1980, *A&A*, 86, 327
 Cantó, J., Tenorio-Tagle, G., & Różyczka, M. 1988, *A&A*, 192, 287
 Colella, P., & Woodward, P. R. 1984, *J. Comput. Phys.*, 54, 174
 Eichler, D. 1982, *ApJ*, 263, 571
 Frank, A., Balick, B., & Livio, M. 1996, *ApJ*, 471, L53
 Frank, A., & Mellema, G. 1996, *ApJ*, 472, 684
 Henize, K. G. 1976, *ApJS*, 30, 491
 Knapp, G. R., Bowers, P. F., Young, K., & Philips, T. G. 1995, *ApJ*, 455, 293
 Parthasarathy, M., & Pottasch, S. R. 1989, *A&A*, 225, 521
 Riera, A., Garcia-Lario, P., Machado, A., Pottasch, S. R., & Raga, A. C. 1995, *A&A*, 302, 137
 Seaquist, E. R., & Davis, L. E. 1983, *ApJ*, 274, 659
 Smith, M. D. 1986, *MNRAS*, 223, 57
 Solf, J. 1994, *A&A*, 282, 567
 Sutherland, R. S., & Dopita, M. A. 1993, *ApJS*, 88, 253
 te Lintel Hekkert, P. 1991, *A&A*, 248, 209
 te Lintel Hekkert, P., & Chapman, J. M. 1996, *A&AS*, 119, 459
 te Lintel Hekkert, P., Chapman, J. M., & Zijlstra, A. A. 1992, *ApJ*, 390, L23
 Tenorio-Tagle, G., Cantó, J., & Różyczka, M. 1988, *A&A*, 202, 256
 Zijlstra, A. A., te Lintel Hekkert, P., Pottasch, S. R., Caswell, J. L., Ratag, M., & Habing, H. J. 1989, *A&A*, 217, 157



FIG. 1.—Proto-planetary nebula He 3-1475 imaged with the *Hubble Space Telescope* WFPC2 through the F658N ([N II] $\lambda 6584$) filter. Image is $15''.9 \times 11''.4$ in size. North is up, and east is to the left.

BORKOWSKI, BLONDIN, & HARRINGTON (see 482, L98)